

Toroidal momentum channeling of geodesic acoustic modes driven by fast ions

This content has been downloaded from IOPscience. Please scroll down to see the full text.

2017 Nucl. Fusion 57 036025

(<http://iopscience.iop.org/0029-5515/57/3/036025>)

View [the table of contents for this issue](#), or go to the [journal homepage](#) for more

Download details:

IP Address: 193.50.135.4

This content was downloaded on 22/02/2017 at 15:59

Please note that [terms and conditions apply](#).

You may also be interested in:

[Physics of intrinsic rotation in flux-driven ITG turbulence](#)

S. Ku, J. Abiteboul, P.H. Diamond et al.

[Overview of toroidal momentum transport](#)

A.G. Peeters, C. Angioni, A. Bortolon et al.

[Rotation and momentum transport in tokamaks and helical systems](#)

K. Ida and J.E. Rice

[On the effect of neoclassical flows on intrinsic momentum in ASDEX Upgrade Ohmic L-mode plasmas](#)

W.A. Hornsby, C. Angioni, E. Fable et al.

[Turbulent momentum transport in core tokamak plasmas and penetration of scrape-off layer flows](#)

J Abiteboul, Ph Ghendrih, V Grandgirard et al.

[Off-diagonal particle and toroidal momentum transport: a survey of experimental, theoretical and modelling aspects](#)

C. Angioni, Y. Camenen, F.J. Casson et al.

[Energetic particle physics in fusion research in preparation for burning plasma experiments](#)

N.N. Gorelenkov, S.D. Pinches and K. Toi

[Consequences of profile shearing on toroidal momentum transport](#)

Y. Camenen, Y. Idomura, S. Jolliet et al.

[Experimental studies of the physical mechanism determining the radial electric field and its radial structure in a toroidal plasma](#)

Katsumi Ida

Toroidal momentum channeling of geodesic acoustic modes driven by fast ions

M. Sasaki^{1,2}, N. Kasuya^{1,2}, K. Itoh^{2,3}, Y. Kosuga^{1,2}, M. Lesur⁴,
K. Hallatschek^{2,5} and S.-I. Itoh^{1,2}

¹ Research Institute for Applied Mechanics, Kyushu University, Kasuga 816-8580, Japan

² Research Center for Plasma Turbulence, Kyushu University, Kasuga 816-8580, Japan

³ National Institute for Fusion Science, Toki 509-5292, Japan

⁴ Institut Jean Lamour, Lorraine University, Vandoeuvre-les-Nancy 54506, France

⁵ Max-Planck-Institute for Plasma Physics, Boltzmannstr. 85748 Garching, Germany

E-mail: sasaki@riam.kyushu-u.ac.jp

Received 2 September 2016

Accepted for publication 15 November 2016

Published 30 January 2017



Abstract

Toroidal momentum channeling by fast ion-driven geodesic acoustic mode (EGAM) is proposed based on a quasi-linear analysis. We focus on a branch due to the magnetic drift resonance. Without the magnetic drift resonance, the eigenfunction of the EGAM has up–down anti-symmetric property in the poloidal direction, and the toroidal momentum flux by the EGAM is zero. If the magnetic drift resonance is considered, the up–down anti-symmetry in the poloidal eigenfunction is violated, and, as a result, the toroidal momentum flux becomes finite. Comparing its magnitude to the other processes such as external momentum input, and the turbulent residual stress, the momentum flux induced by the EGAM is found to be significant in the total momentum balance. This suggests that EGAMs can be used as a control knob for the toroidal rotation.

Keywords: geodesic acoustic mode, energetic particle, momentum flux, toroidal rotation

(Some figures may appear in colour only in the online journal)

1. Introduction

Toroidal rotation plays important roles in suppressing of turbulent transport [1] as well as stabilizing magnetohydrodynamic instability such as resistive wall modes [2]. The generation mechanisms of the toroidal rotation have been subjects to intensive research, and the concept of the non-diffusive momentum transport is now well established. The off-diagonal momentum flux [3, 4] and the origins of spontaneous rotation have been investigated. The residual stress due to drift wave and ITG turbulence has been reported as the origin of the intrinsic rotation [5–9].

In this paper, we show that energetic particle (EP)-drive modes can play a role in the non-diffusive momentum transport. In the literature, energy channeling from EP to bulk plasma has been studied, and processes such as α -channeling and GAM channeling have been proposed [10, 11]. Whether the EP driven modes can contribute to the momentum transport or not is crucial. If it is possible, they may be promising

control knobs for the toroidal rotation, because the EP-driven modes are controllable externally [21]. Energetic particle-driven geodesic acoustic modes (EGAMs) are one of the EP driven modes. EGAMs are excited by wave-particle resonances with EPs [12–15]. Nonlinear processes such as frequency chirping, saturation, mode coupling, and subcritical instabilities have been reported [16–20]. Recently, large amplitude of EGAM was observed in experiments, where the amplitude of the potential perturbation normalized by the electron temperature was observed to be order of unity [21]. Impacts of the EGAM on the background plasma are expected to be significant.

In this study, we investigate the toroidal momentum transport due to EGAMs, based on a quasi-linear analysis. The EGAMs have several branches; the eigenfrequency of each branch is close to either the standard GAM frequency $\omega_G \sim c_s/R$ (c_s is the sound speed, R is the major radius of the plasma), the transit frequency of EP, or the magnetic drift frequency of EP. We focus on the third branch, which is due to

the magnetic drift of EP [15]. The parallel momentum flux is calculated based on the poloidal eigenfunction of the EGAM, and its magnitude is shown to be significant in the total momentum balance of bulk plasmas. The paper is organized as follows. In the next section, the poloidal eigenmodes of the EGAM is described. In section 3, the spatial structures of the velocity field of the EGAM is derived, and the quasi-linear parallel momentum flux is evaluated. The summary is given in section 4.

2. Poloidal eigenmode of EGAM

In this section, the poloidal eigenmode analysis of EGAM is briefly described, and the poloidal structure of the eigenfunction is explained. In this paper, time and space are normalized by v_T/R and the ion gyroradius, respectively, where v_T is the ion thermal velocity, and R is the major radius. The velocity is normalized by v_T , the electrostatic potential is normalized by e/T_i , and the density of the fast ions are normalized by that of the electrons.

We consider a simple tokamak equilibrium with circular magnetic surfaces. We neglect effects of trapped particles due to magnetic inhomogeneity, which is justified when the mode frequency is much larger than the bounce frequency of trapped particles. The velocity distribution function of the bulk ions is assumed to be Maxwellian. For transparency of the analysis, the fast ions' distribution is taken as a beam type distribution [15], where the speed of the fast ions is given by u_0 , and the pitch angle defined as the parallel velocity normalized by the total velocity is Λ_0 , and the density of the fast ions is n_h . Here we use the following ordering; $u_0 \gg 1, n_h \ll 1$. Based on the assumptions above, the electrostatic EGAM is considered.

The gyrokinetic equation for the fast ions has two kinds of resonances in accordance with the transit frequency and the magnetic drift frequency of the fast ions. The transit frequency and the magnetic drift frequency are introduced as $\omega_h = u_0 \Lambda_0 / q$ and $\omega_D = k_r u_0^2 (1 + \Lambda_0^2) / 2$, respectively. Here, q is the safety factor, and k_r is the radial wavenumber of the GAM, which is treated as the smallness parameter, $k_r \ll 1$. Thus, the dominant resonance depends on the velocity and the pitch angle of the fast ions. (i): in the limit where the transit frequency of the fast ions is much larger than the drift frequency, $\omega_h \gg \omega_D$, the resonance due to the transit frequency becomes important, and the solution with $\omega \sim \omega_h$ appears [12, 14, 22–24]. (ii): in the limit where the resonance due to the drift frequency becomes dominant, $\omega_h \ll \omega_D$, a solution with a frequency close to the drift frequency of the fast ions appears, $\omega \sim \omega_D$ [15]. This limit is valid when $u_0 \gg 2\Lambda_0 \{k_r q (1 + \Lambda_0^2)\}$. In this limit, the eigenmode equation is given as

$$\sum_{\nu=-\infty}^{\infty} D_{\mu,\nu} \phi_\nu = 0, \quad (1a)$$

$$D_{\mu,\nu} = \delta_{\mu,\nu} \{ \tau (1 - \delta_{\mu,0}) + 1 \} - (H_{\mu-\nu} + I_{\nu,\mu-\nu}), \quad (1b)$$

where μ is an integer ($\mu = -\infty, \dots, \infty$), and $\delta_{\mu,\nu}$ is the Kronecker delta. The detailed derivation of this dispersion

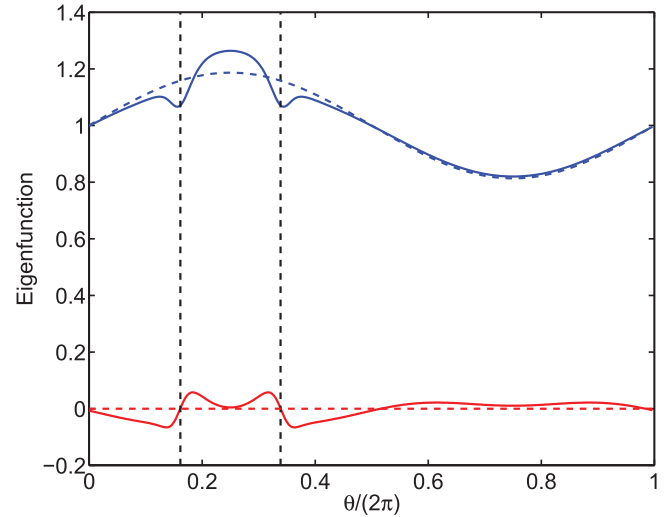


Figure 1. Poloidal eigenfunction of the electrostatic potential perturbation in the case of $q = 3, \tau = 0.5, k_r = 0.12, n_h = 0.015, \Lambda_0 = 0.1, u_0 = 5$. The eigenfunction in the limit without the magnetic drift resonance, equation (4), is also shown as a dashed curve. The eigenfunction has bumps and the imaginary part appears near the resonance locations.

relation is written in [15]. The first term in equation (1b) stems from adiabatic response of the electron and the bulk ions, $I_{\nu,\mu-\nu}$ is the contribution from the non-adiabatic response of the bulk ions, which includes the Landau damping. The non-adiabatic responses of fast ions is denoted by $H_{\mu-\nu}$, which includes the effect of resonance due to the magnetic drift as

$$\omega - \omega_D \sin \theta = 0. \quad (2)$$

The expressions of $I_{m,l}$ and H_l are given in appendix A. The dispersion relation equation (1a) has solutions such as the ion sound waves, and the standard GAM, whose frequency is given as

$$\omega_G = \sqrt{\left(\frac{7}{4} + \frac{1}{\tau}\right) \left[1 + \frac{46\tau^2 + 32\tau + 8}{(7\tau + 4)^2 q^2}\right]}, \quad (3)$$

in the large safety factor limit [25]. In addition to these, a branch whose frequency corresponds to ω_D is obtained. When $\omega_G > \omega_D$, the solution with $\omega \approx \omega_D$ is unstable. The solution with $\omega \approx \omega_G$ becomes unstable when $\omega_G < \omega_D$. The growth rate of the unstable branch becomes maximum when $\omega_G = \omega_D$. A detailed description of the eigenfrequency is given in [15].

We focus on the branch with $\omega \approx \omega_D$ in this paper. The poloidal harmonics of the electrostatic potential, ϕ_m , can be obtained from the eigenequation equation (1a), and the poloidal structure of the potential can be calculated from $\phi_\omega = \sum_m \phi_m e^{im\theta}$, which is shown in figure 1. Since we consider the poloidally inhomogeneous resonance, equation (2), there are special values of the poloidal angle (resonance locations), $\theta_* = \arcsin(\omega/\omega_D)$, where the resonance condition is satisfied. The potential eigenfunction has bumps and the imaginary part appears (which corresponds to the phase shift) at the resonance locations $\theta \approx \theta_*$. In the limit where we neglect the magnetic drift resonance and the poloidal modes are truncated at $m = \pm 1$, the potential eigenfunction can be written as

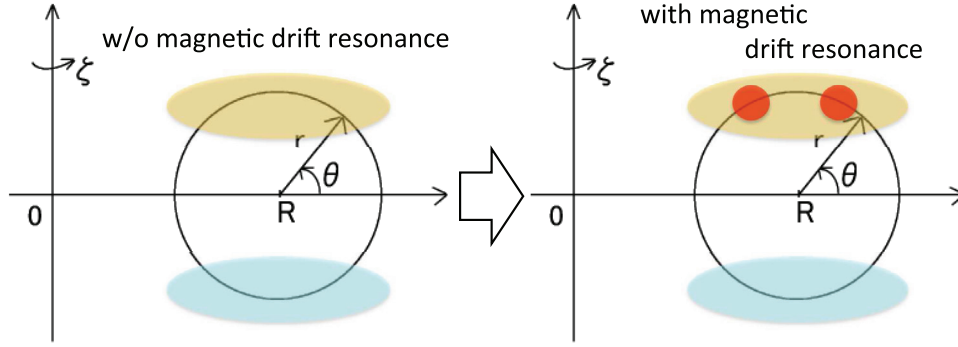


Figure 2. Schematic figure of the eigenfunction of the electrostatic potential perturbations with and without the magnetic drift resonance. The up–down anti-symmetry of the eigenfunction is broken due to the magnetic drift resonance.

$$\phi_\omega = \left[1 + \frac{k_r}{\omega\tau} \sin\theta \right] \phi_0, \quad (4)$$

which agrees with the previous studies [26]. Here, ϕ_0 is the poloidal averaged potential amplitude. In this limit, this eigenfunction has no bumps and no phase shift, and satisfies the up–down anti-symmetry in the poloidal cross section. The up–down anti-symmetry is broken due to the magnetic drift resonance, which is illustrated in a schematic view as figure 2. In the case of positive k_r , the resonance locations are in the upper side of the poloidal cross section. In the case of the negative k_r , the resonance locations are in the lower side, as seen from the resonance condition equation (2).

3. Quasi-linear parallel momentum flux

In this section, the toroidal momentum flux by the EGAM is described. Based on the eigenmode analysis shown in the previous section, the poloidal structure of the velocity field, $v_{r,\omega}, v_{\parallel,\omega}$ (the radial velocity, and the parallel velocity perturbations), is calculated. Then, by using the expressions of the velocity perturbations, the toroidal momentum flux is derived in the framework of the quasi-linear theory. Finally, the magnitude of the momentum flux induced by the magnetic drift resonance is compared with this induced by other processes, such as turbulence effects and the collisional momentum transfer from the fast ions to the bulk ions.

3.1. Poloidal structure of momentum flux

The parallel momentum flux by the GAM is defined as

$$\Pi_{r\parallel} = \text{Re}[v_{r,\omega}^* v_{\parallel,\omega}]. \quad (5)$$

Since the toroidal mode number of the GAM is zero, the symmetry breaking of the parallel wavenumber spectrum is not necessary unlike in the case of the intrinsic torque by turbulence [5, 6, 8]. So, the poloidal structures of the velocity perturbations are important to determine the momentum flux in the case of the GAM.

The radial velocity fluctuation is calculated from the $E \times B$ drift velocity, and the parallel velocity fluctuation, $v_{\parallel,\omega}$, is

obtained by taking the moment of the velocity distribution of the bulk ion, $\delta f_\omega^{(i)}$, as

$$v_{r,\omega} = -\frac{1}{r} \partial_\theta \phi_\omega, \quad (6)$$

$$\begin{aligned} v_{\parallel,\omega} &= \int v_{\parallel} \delta f_\omega^{(i)} d^3v \\ &= \sum_{m=-\infty}^{\infty} \phi_m e^{im\theta} \sum_{l=-\infty}^{\infty} u_{m,l} e^{il\theta}, \end{aligned} \quad (7)$$

where the coefficient $u_{m,l}$ is given in appendix B. If we neglect the magnetic drift resonance and truncate the poloidal modes at $m = \pm 1$, the expressions of the parallel and the radial velocity fluctuations are reduced to

$$v_{\parallel,\omega} = -i \frac{k_r \phi_0}{q\omega^2} \left(\frac{1}{2\tau} + 1 \right) \cos\theta, \quad (8)$$

$$v_{r,\omega} = -\frac{k_r \phi_0}{r\omega\tau} \cos\theta, \quad (9)$$

which agree with the previous theories. The poloidal structures of the velocity fluctuations of the branch due to the magnetic drift resonance are shown in figure 3. Around the resonance locations, steep structures appear, and the magnitudes of the real and imaginary parts are comparable, which indicates a large phase shift. In particular, at the resonance locations, the magnitude of the radial velocity is enhanced several times compared to that without the magnetic drift resonance. Except near the resonance locations, the eigenfunctions of the parallel and radial velocities have similar structures with equations (8) and (9), respectively. In order to clarify the phase relation between the parallel and radial velocities, the time evolution of their poloidal structures are calculated from $v_{\parallel}(\theta, t) = \text{Re}[v_{\parallel,\omega} e^{-i\omega t}]$, $v_r(\theta, t) = \text{Re}[v_{r,\omega} e^{-i\omega t}]$, which are shown in figure 4. The poloidal propagation can be seen around the resonance locations, while the eigenfunctions exhibit the standing wave patterns except around the resonance locations. It is clearly seen that the parallel and radial velocities are in phase only around the resonance locations. This phase relation around the resonance location is completely different

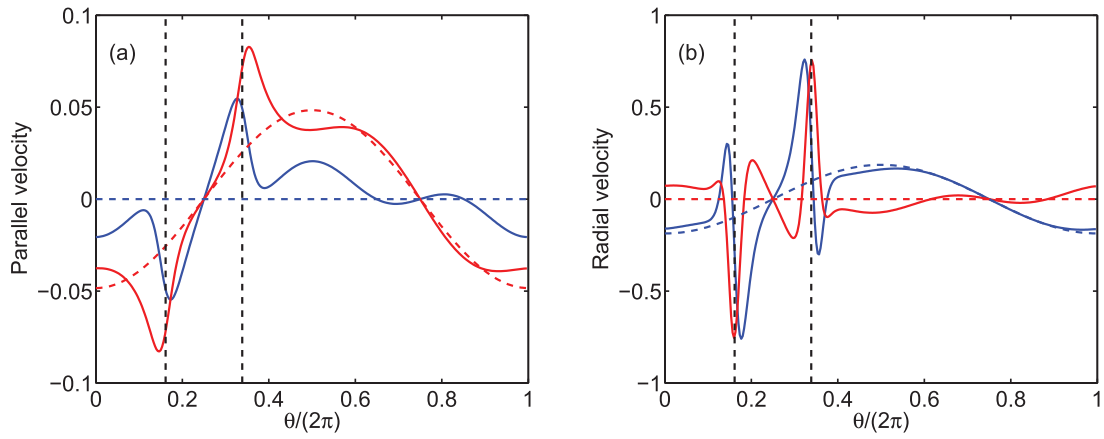


Figure 3. Poloidal eigenfunction of the parallel and radial velocity perturbations in the case of $q = 3$, $\tau = 0.5$, $k_r = 0.12$, $n_h = 0.015$, $\Lambda_0 = 0.1$, $u_0 = 5$. For the radial velocity, $r v_{r,\omega}$ is plotted. The eigenfunctions in the limit without the magnetic drift resonance are also shown as a dashed curve. The dashed black lines correspond to the resonance locations.

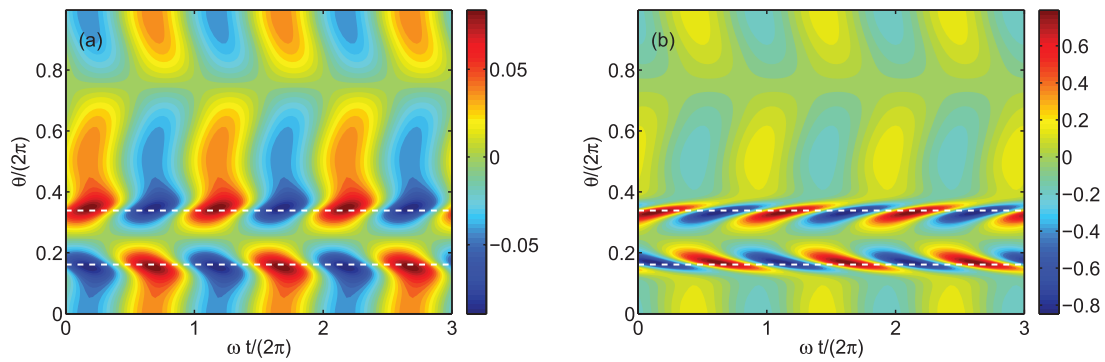


Figure 4. Time evolution of the poloidal structures of the (a) parallel and (b) radial velocity perturbations. The dashed white lines correspond to the resonance locations. For the radial velocity, $r v_{r,\omega}$ is plotted.

from the eigenfunctions in the limit without the magnetic drift resonance.

The parallel momentum flux is obtained from equations (5)–(7), which is shown in figure 5. The unit of the momentum flux is the square of the ion thermal velocity. The momentum flux is localized around the resonance locations. The localization of the flux can be understood as follows. Around the resonance locations, the radial and parallel velocities are in phase as shown in figure 4, which leads to the positive momentum flux. Except near the resonance locations, their phase difference is $\pi/2$ so that the momentum flux becomes zero in this region. If we neglect the magnetic drift resonance and the poloidal modes are truncated at $m = \pm 1$, the eigenfunction of the potential shows up–down anti-symmetry as shown in figure 2. In this limit, the phase difference between the radial and parallel velocities is $\pi/2$ in the entire region, so that the parallel momentum flux becomes zero. Breaking of the up–down anti-symmetry of the poloidal eigenfunction, which is due to the magnetic drift resonance, is essential for getting the finite momentum flux. The poloidally averaged momentum flux, $\langle \Pi_{r\parallel} \rangle$, is evaluated in the dimensional form as

$$\langle \Pi_{r\parallel} \rangle \sim 10^{-3} \text{sgn}(B) \rho_* \left| \frac{e\phi_0}{T_i} \right|^2 v_T^2, \quad (10)$$

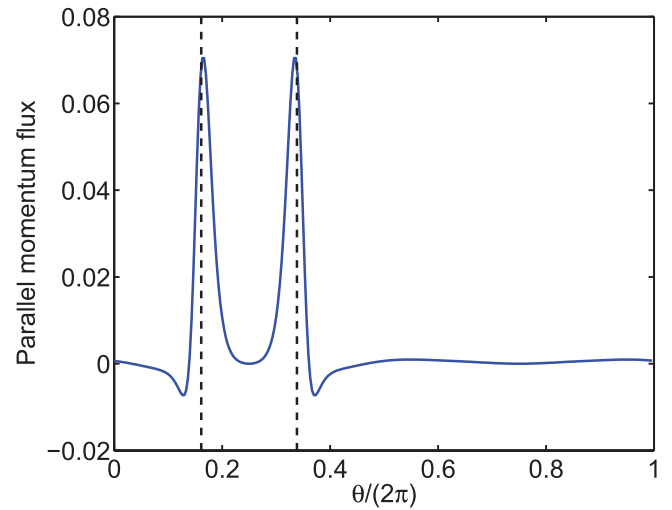


Figure 5. Poloidal structure of the parallel momentum flux by EGAM.

where $\text{sgn}(B)$ is the sign of the magnetic field, v_T is the ion thermal velocity, and ρ_* is defined as $\rho_* = \rho/r$. The sign of the momentum flux depends only on that of the magnetic field. In order to clarify the origin of the sign of the momentum flux, the relation of the parallel momentum flux with the ion heating rate by the GAM is discussed below. The ion heating

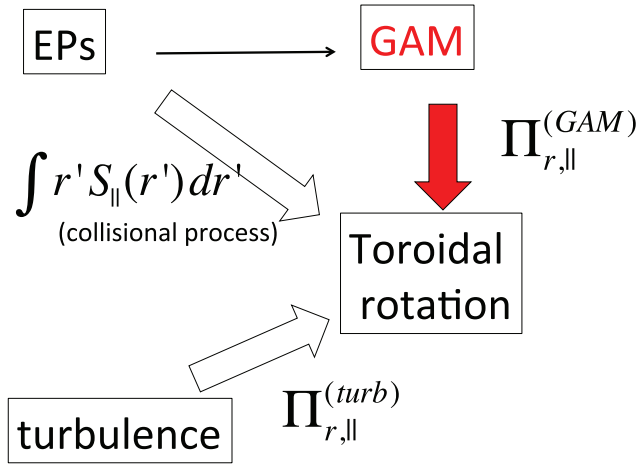


Figure 6. Schematic view of toroidal momentum channeling by EGAM.

rate is evaluated by the product of the current perturbation \mathbf{J}_ω with the electric field perturbation \mathbf{E}_ω as [15]

$$\text{Re}[\mathbf{J}_\omega \cdot \mathbf{E}_\omega^*] \approx -2\text{Re}\left[\int q^{-1}v_{\parallel}\delta f_\omega^{(i)}d^3v\partial_\theta\phi_\omega^*\right]. \quad (11)$$

The ion heating rate of the EGAM which we focus on is analyzed in [15]. It has a poloidal structure similar to the parallel momentum flux. By using the expression of the ion heating rate equation (11), the parallel momentum flux can be rewritten as

$$\Pi_{r,\parallel} \approx \text{sgn}(B)\frac{q}{r}\text{Re}[\mathbf{J}_\omega \cdot \mathbf{E}_\omega^*]. \quad (12)$$

Since the ion heating rate is always positive in the case of linearly unstable EGAM [15], the sign of the parallel momentum flux is determined only by that of the magnetic field.

3.2. Momentum channeling by EGAM

In this section, the magnitude of the momentum flux is discussed, comparing that induced by the EGAM with that induced by the other processes. Here we consider the intrinsic torque by the turbulence [5] and the collisional momentum transfer from the fast ions to the bulk ions. The radial shear of the mean parallel velocity, V'_{\parallel} in a stationary state is evaluated as [5]

$$V'_{\parallel} = \frac{\Pi_{r,\parallel}^{(\text{turb})} + \Pi_{r,\parallel}^{(\text{GAM})}}{\chi_\phi} - \frac{1}{\chi_\phi r} \int r S_{\parallel}(r) dr, \quad (13)$$

where $\Pi_{r,\parallel}^{(\text{turb})}$ is the momentum flux by the turbulence, $\Pi_{r,\parallel}^{(\text{GAM})}$ is the momentum fluxes due to the GAM, χ_ϕ is the turbulent diffusion coefficient, and S_{\parallel} is the momentum source, which is due to the collisional momentum transfer from the fast ions. The processes we consider is summarized in figure 6.

First, the comparison with the momentum source term is described. The momentum source term is estimated as

$$\frac{1}{r} \int r S_{\parallel}(r) dr = \frac{1}{r} \int r \nu_{ih} u_0 \Lambda_0 dr. \quad (14)$$

Here, ν_{ih} is the collision frequency between the bulk and the fast ions. The ratio of the momentum flux by the GAM with the collisional momentum transfer is evaluated as

$$\left| \frac{\Pi_{r,\parallel}^{(\text{GAM})}}{r^{-1} \int r S_{\parallel}(r) dr} \right| \sim \frac{10^{-3} \rho_*^2}{\nu_{ih} u_0 \Lambda_0} |\phi_0|^2. \quad (15)$$

This ratio becomes order of unity when the amplitude of the GAM is large $\phi_0 \sim 1$. For instance, when $\rho_* = 10^{-2}$, $\nu_{ih} = 10^{-8}$ and $\phi_0 = 1$, the ratio becomes unity. Hence, the parallel momentum flux due to EGAM can not be neglected compared to the collisional momentum input from the fast ions.

Next, a comparison with the intrinsic torque by the turbulence is shown. The momentum flux due to the turbulence is evaluated as [9]

$$\Pi_{r,\parallel}^{(\text{turb})} \sim -\rho_* \frac{qR}{\hat{s}} \frac{1}{2c_s} \chi_i \frac{1}{L_T^2}, \quad (16)$$

where L_T is the scale length of the temperature profile. The ratio of the momentum flux by the GAM with that by the turbulence can be estimated as

$$\left| \frac{\Pi_{r,\parallel}^{(\text{GAM})}}{\Pi_{r,\parallel}^{(\text{turb})}} \right| \sim 10^{-3} \rho_*^{-2} \frac{\hat{s} L_T}{qR} |\phi_0|^2. \quad (17)$$

Here, the thermal diffusion coefficient χ_i is estimated as the gyro-Bohm diffusion $\chi_i \sim v_T \rho_i^2 / L_T$. This ratio also becomes order of unity when the amplitude of the GAM is large $\phi_0 \sim 1$. In the case that $\rho_* = 10^{-2}$, $L_T/R = 0.3$, $q = 3$, $\hat{s} = 1$, $\phi_0 = 1$, this ratio becomes unity. Therefore, EGAMs can play an important role of momentum channeling from the fast ions to the bulk ions. This process would have a substantial impact on the generation of the toroidal rotation.

4. Summary

Toroidal momentum channeling by EGAM is proposed in the framework of the quasi-linear theory. A branch due to the magnetic drift resonance is focused on, and the eigenfunctions of the electrostatic potential and the velocity field is calculated. The eigenfunction of the electrostatic potential has up-down anti-symmetric property in the poloidal direction without the magnetic drift resonance, and the toroidal momentum flux by the EGAM is zero. If the magnetic drift resonance is considered, the up-down anti-symmetry in the poloidal eigenfunction is violated, and the toroidal momentum flux becomes finite. Comparing its magnitude to the other processes such as the externally momentum input, and the turbulent residual stress, the momentum flux by the EGAM is found significant in the total momentum balance. This suggests that EGAMs may be used as control knobs for the toroidal rotation.

Acknowledgments

This work was partly supported by a grant-in-aid for scientific research of JSPS, Japan (JP16K18335, JP16H02442,

JP15H02335, JP15H02155, JP24740372, JP21224014) and by the collaboration programs of NIFS (NIFS14KNST072, NIFS15KNST089) and of the RIAM of Kyushu University, and Asada Science foundation.

Appendix A. Expressions of $I_{m,l}$ and H_l

The expressions of $I_{m,l}$ is given as

$$I_{m,l=0} = -\left(1 - \frac{k_r^2}{2}\right) \frac{q\omega}{m} Z\left(\frac{q\omega}{m}\right) - \frac{k_r^2 q^2}{4} (\alpha_{m-1} + \alpha_{m+1} - 2\alpha_m), \quad (\text{A.1a})$$

$$I_{m,l=\pm 1} = i \frac{k_r q}{2} (\beta_{m\pm 1} - \beta_m), \quad (\text{A.1b})$$

and $I_{m,|l|>1}$ is neglected, which corresponds to keeping terms up to the ordering of k_r^2 . Here, $Z(x)$ is the plasma dispersion function. The functions α_m and β_m for $m \neq 0$ are introduced as

$$\alpha_m = \left(\frac{q\omega}{m}\right)^2 + \left\{ \left(\frac{q\omega}{m}\right)^3 + \frac{q\omega}{m} + \frac{m}{2q\omega} \right\} Z\left(\frac{q\omega}{m}\right), \quad (\text{A.2a})$$

$$\beta_m = \frac{q\omega}{m} + \left\{ \left(\frac{q\omega}{m}\right)^2 + \frac{1}{2} \right\} Z\left(\frac{q\omega}{m}\right). \quad (\text{A.2b})$$

These functions at $m = 0$ are defined as $\alpha_{m=0} = -3/2$ and $\beta_{m=0} = 0$. The expression of $I_{m,l}$ has terms related to the plasma dispersion function, which causes the Landau damping. The expression of H_l is

$$H_l = \oint 2n_n J_0(kv_{\perp,h})^2 k_r \frac{\omega \sin \theta e^{-i\theta}}{(\omega - \omega_D \sin \theta)^2} \frac{d\theta}{2\pi}. \quad (\text{A.3})$$

Here, this integral has the resonance due to the magnetic drift resonance as in equation (2), which can destabilize the EGAMs [15].

Appendix B. Expressions of $u_{m,l}$

The expressions of $u_{m,l}$ is given as

$$u_{m,l=0} = -\frac{q\omega}{m} \left\{ 1 + \frac{q\omega}{m} Z\left(\frac{q\omega}{m}\right) \right\} + k_r^2 q^2 \times \left(\frac{q\omega}{2m} \alpha_m - \frac{1}{4} \frac{q\omega}{m-1} \alpha_{m-1} - \frac{1}{4} \frac{q\omega}{m+1} \alpha_{m+1} \right) - \frac{3k_r^2 q^3 \omega}{8} \left(\frac{1}{m-1} + \frac{1}{m+1} - \frac{2}{m} \right),$$

$$u_{m,l=\pm 1} = i \frac{k_r q}{2} \left(\frac{q\omega}{m \pm 1} \beta_{m \pm 1} \mp \frac{q\omega}{m} \beta_m \right),$$

where α_m and β_m are given in equations (A.2a) and (A.2b), respectively. When $m = 0, \pm 1$, $u_{m,l}$ is expressed as

$$u_{0,l=0} = \frac{k_r^2 q^2}{4} q\omega (\alpha_{-1} - \alpha_1),$$

$$u_{0,l=\pm 1} = \pm i \frac{k_r q}{2} q\omega \beta_{\pm 1},$$

$$u_{\pm 1,l=0} = \mp q\omega (1 \pm q\omega Z(\pm q\omega)) + k_r^2 q^2 \left(\frac{q\omega}{2} \alpha_{\pm 1} \mp \frac{q\omega}{8} \alpha_{\pm 2} \right),$$

$$u_{\pm 1,l=\mp 1} = i \frac{k_r q}{2} q\omega \beta_{\pm 1},$$

$$u_{\pm 1,l=\pm 1} = \pm i \frac{k_r q}{2} \left(\frac{q\omega}{2} \beta_{\pm 2} - q\omega \beta_{\pm 1} \right).$$

References

- [1] Biglari H., Diamond P.H. and Terry P.W. 1990 *Phys. Fluids B* **2** 1
- [2] Betti R. and Freidberg J.P. 1995 *Phys. Rev. Lett.* **74** 2949
- [3] Shaing K.C. 2001 *Phys. Plasmas* **8** 193
- [4] Ida K., Miura Y., Matsuda T., Itoh K., Hidekuma S., Itoh S.-I. and JFT-2M Group 1995 *Phys. Rev. Lett.* **74** 1990
- [5] Diamond P.H., McDevitt C.J., Gurcan O.D., Hahm T.S. and Naulin V. 2008 *Phys. Plasmas* **15** 012303
- [6] Gurcan O.D., Diamond P.H., Hahm T.S. and Shingh R. 2007 *Phys. Plasmas* **14** 042306
- [7] Wang W.X., Hahm T.S., Ethier S., Rewoldt G., Lee W.W., Tang W.M., Kaye S.M. and Diamond P.H. 2009 *Phys. Rev. Lett.* **102** 035005
- [8] McDevitt C.J., Diamond P.H., Gurcan O.D. and Hahm T.S. 2009 *Phys. Rev. Lett.* **103** 205003
- [9] Kosuga Y., Diamond P.H. and Gurcan O.D. 2010 *Phys. Plasmas* **17** 102313
- [10] Fisch N.J. and Herrmann M.C. 1994 *Nucl. Fusion* **34** 1541
- [11] Sasaki M., Itoh K. and Itoh S.-I. 2011 *Plasma Phys. Control. Fusion* **53** 085017
- [12] Fu G.Y. 2008 *Phys. Rev. Lett.* **101** 185002
- [13] Qiu Z., Zonca F. and Chen L. 2010 *Plasma Phys. Control. Fusion* **52** 095003
- [14] Berk H.L. and Zhou T. 2010 *Nucl. Fusion* **50** 035007
- [15] Sasaki M., Kasuya N., Itoh K., Hallatschek K., Lesur M., Kosuga Y. and Itoh S.-I. 2016 *Phys. Plasmas* **23** 102501
- [16] Wang H., Todo Y. and Kim C.C. 2013 *Phys. Rev. Lett.* **110** 155006
- [17] Zarzoso D., Garbet X., Sarazin Y., Dumont R. and Grandgirard V. 2012 *Phys. Plasmas* **19** 022102
- [18] Zarzoso D. et al 2013 *Phys. Rev. Lett.* **110** 125002
- [19] Lesur M., Itoh K., Ido T., Osakabe M., Ogawa K., Shimizu A., Sasaki M., Ida K., Inagaki S., Itoh S.-I. and LHD Experimental Group 2016 *Phys. Rev. Lett.* **116** 015003
- [20] Ido T. et al and LHD Experimental Group 2016 *Phys. Rev. Lett.* **116** 015002
- [21] Ido T. et al and The LHD Experiment Group 2015 *Nucl. Fusion* **55** 083024
- [22] Girardo J.B., Zarzoso D., Dumont R., Garbet X., Sarazin Y. and Sharapov S. 2014 *Phys. Plasmas* **21** 092507
- [23] Zarzoso D., Biancalani A., Bottino A., Lauber P., Poli E., Girardo J.B., Garbet X. and Dumont R.J. 2014 *Nucl. Fusion* **54** 103006
- [24] Miki K. and Idomura Y. 2015 *Plasma Fusion Res.* **10** 3403068
- [25] Sugama H. and Watanabe T.-H. 2006 *J. Plasma Phys.* **72** 825
- [26] Sasaki M., Itoh K., Ejiri A. and Takase Y. 2009 *J. Plasma Phys.* **75** 721